Department of Electrical
and
Computer Systems Engineering

Technical Report
MECSE-14-2004

FDTD simulation of mode-locked fiber lasers

Lam Quoc Huy

MONASH
UNIVERSITY

FDTD simulation of mode-locked fiber lasers

Lam Quoc Huy & Le Nguyen Binh
Department of Electrical and Computer Systems Engineering
Monash university, Clayton, Victoria 3168, Australia

Abstract

This paper presents a novel temporal domain simulation for studying the generation and propagation of photonic pulses in mode-locked lasers. The pulse propagation equation has been solved fully in time domain using finite difference method (FDTD) without the need of conversion of optical signals into frequency domain. Unlike other published works on the modeling of mode-locked lasers where only partial pulse sequence could be represented, in this work the complete pulse sequence can be generated in harmonic mode-locked fiber lasers has been simulated using this FDTD approach. To the best of our knowledge, the simulation of the whole pulse train in such laser is demonstrated for the first time. The propagation of an optical pulse through an optical fiber has been simulated and compared to the analytical results to ensure the validity of the numerical approach. The pulse formation in a harmonic mode-locked fiber laser has been simulated. The effects of the laser cavity settings on the characteristics of the mode-locked pulses have been studied and the simulated results have shown consistency with the experimental results which have also been reported in another report posted on this website.

1 Introduction

Generation of ultra-short optical pulses with multiple gigabits repetition rate is critical for ultra-high bit rate optical communications, particularly for the next generation of terabits/sec, optical fiber systems. In addition, the field of optical packet switching has gained recognition in recent years and requires very short and high peak power pulse generators to provide all optical switching. Recent reports on the generation of short pulse trains at repetition rates in the order of 40 Gb/s show that active mode-locked fiber lasers are the potential sources of such pulse trains [1-5]. Therefore it is

important to develop theoretical models and simulation techniques to analyze the performance and characteristics of these lasers.

Prior works for studying the propagation of photonic pulses in optical fibers and the formation of optical pulse in active mode-locked fiber lasers have been largely based on the nonlinear Schodinger (NLS) equation [6-8]. The most popular method used for solving the propagation of the pulse in an optical fiber is the well known split-step Fourier (SSF) [6]. In which the equation can be split into two parts: the linear and nonlinear parts. The linear part is solved in frequency domain by taking the Fourier transform. The resultants are then converted back to time domain by taking the inverse Fourier transform. The nonlinear part is solved in time domain.

The SSF is claimed to be a fast method for studying the propagation of pulse in fiber and has been applied to study the formation of a single pulse in an active mode-locked laser [6-11]. However, since SSF requires converting signal from time domain into frequency domain by using Fast Fourier Transform (FFT) algorithm, the signal must be windowed and the number of samples in the window must be limit. Although each FFT operation is relatively fast, a large number of FFT operations on a large-size array make the computation impossible.

This paper presents a novel approach of simulation in which the propagation of the pulse envelops through all photonic components in the laser cavity is analyzed fully in temporal domain. The linear dispersion and nonlinear self phase modulation has been approximated accurately using the finite difference method. Indeed simulated results have been compared and confirmed with those obtained analytically and experimentally.

This paper is organized as following: Section 2 outlines the temporal domain representation of the laser model, the optical filter, the EDFA, the fiber and the optical modulator. Section 3 described the mathematical models using finite difference approach for all these elements. Simulation results are then presented firstly for the propagation of light pulses through an optical fiber to demonstrate the validity of our modeling technique. Models of other photonic elements are then integrated with the fiber propagation model to form a generic simulation package for generation of mode-locked pulses. The simulation results are presented in Section 4. The effects of the modulation frequency, modulation depth, filter bandwidth and pump power on the

generated pulses are studied and confirmed with experimental observations. Simulation of the generation and mode-locking of pulses in a rational harmonic mode-locked laser is also demonstrated.

2 The laser model

The laser is modeled as shown in Figure 1. All optical and photonic components are indicated and the signal flow paths are noted by straight lines with arrowed end. The model consists of an EDFA, which is the gain medium for the laser, a length of optical fiber of dispersion shifted type (DSF), an optical filter BPF, and an optical intensity modulator. The optical waves are amplified in the EDFA and then propagate through the DSF. The lightwaves intensity is then modulated by the optical modulator. The BPF ensures that a certain optical frequency band is allowed to pass through, hence this determines the central wavelength and the pulse width of the generated signals. The output of the modulator is fed back into the EDFA to create a loop. The signals are then circulating through the optical loop. The detail modeling of each photonic component of the cavity is described in the following sections.

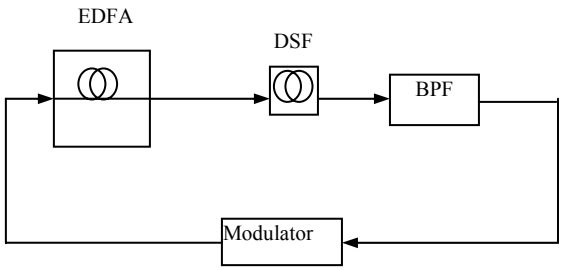

Figure 1 – General schematic model of the fiber laser

2.1 The fibre wave propagation equation

The fiber can be modeled by the propagation equation [8]

$$\frac{\partial A}{\partial z} + \frac{j}{2}\beta_2 \frac{\partial^2 A}{\partial T^2} + \frac{\alpha}{2} A = j\gamma |A|^2 A \qquad (1)$$

where A is the signal envelope, z is the axial distance, T is the delayed time ($T = t - z/v_g$), v_g is group velocity, α is the linear attenuation factor of the fiber and accounts for the loss, γ is the nonlinear coefficient which accounts for the self phase

modulation effect, β_2 is the second order derivative of the propagation constant β and can be calculated from the fiber dispersion parameter as

$$\beta_2 = -\frac{\lambda^2 D}{2\pi c} \tag{2}$$

in which λ is the operating wavelength in vacuum, D is the dispersion factor of the fiber, c is the speed of light.

2.2 Modeling of the EDFA

The EDFA can be modeled by an EDF with ions pumped into excited state for providing gain when the signal travels through it. The propagation equation for the signal traveling through the EDF is [8]

$$\frac{\partial A}{\partial z} + \frac{j}{2}\left(\beta_2 + j g_0 T_2^2\right)\frac{\partial^2 A}{\partial T^2} + \frac{1}{2}(g_0 - \alpha)A = j\gamma|A|^2 A \tag{3}$$

This equation follows the similar form of (*1*) except that the gain factors g_0 and T_2 are included. The T_2 term accounts for the decrease of the gain coefficient at the wavelength located far from the gain peak and is usually defined as the inverse of the 3 dB bandwidth of the gain spectrum. The saturation of the EDFA is usually modeled by presenting g_0 as a function of the signal average power

$$g_0 = \frac{g_{ss}}{1 + P_{av}/P^{sat}} \tag{4}$$

where g_{ss} is small signal gain, P_{av} is the signal average power, P^{sat} is the saturation power level.

2.3 The optical modulator

The modulator can be modeled from the transmission function

$$T = \alpha_m \cos^2\left(\frac{\pi(v_m - V_{sh})}{2V_\pi}\right) \tag{5}$$

where V_π is the voltage applied into the modulator causes π phase shift in one arm of the integrated optical interferometer, V_{sh} accounts for the DC drift of the modulator, α_m is the insertion loss, v_m is the modulating voltage signal and can be given by

$$v_m = V_m cos(\omega_m t) + V_b \quad (6)$$

in which V_m is the amplitude of the modulating signal, ω_m is the modulating frequency, V_b is the bias voltage.

Substituting (6) into (5) and note that V_{sh} can be assumed to be zero without any affect to the final result, the transmission function of the modulator can be written as

$$T = \alpha_m \cos^2\left(\frac{\pi}{4}\Delta_m \cos(\omega_m t) + \frac{\pi}{2}\frac{V_b}{V_\pi}\right) \quad (7)$$

where $\Delta_m = 2V_m/V_\pi$ is the modulation depth. When the modulation is biased at the quadrature point $V_b = V_\pi/2$, (7) becomes

$$T = \alpha_m \cos^2\left[\frac{\pi}{4}(\Delta_m \cos(\omega_m t) + 1)\right] \quad (8)$$

2.4 The optical filter model

The optical filter BPF can be described by the following transfer function following a Gaussian profile as

$$H(f) = \alpha_F \exp\left(-\frac{1}{2}\left(\frac{f}{B_0}\right)^2\right) \quad (9)$$

where α_F is the insertion loss, B_0 is half of the $(1/e)$ bandwidth of the filter

3 Numerical analysis of the model

To simulate every pulses that exist in a harmonic mode-locked laser without windowing, a fully time domain method is used here. The propagation equations of the pulses in the optical fiber are solved using finite element method.

Firstly, the propagation equation of the pulse in the EDF is solved to obtain the signal at the output of the EDF. The time and space are discretized by using the following equations

$$z = k\Delta z \quad (10)$$

$$T = m\Delta T \quad (11)$$

where Δz and ΔT are the step in space domain and time domain respectively, k and m are integers. The derivatives of A in Eq. (3) can be approximated as following

$$\frac{\partial A(z,T)}{\partial z} = \frac{A_{k+1,m} - A_{k,m}}{\Delta z} \tag{12}$$

$$\frac{\partial A(z,T)}{\partial T} = \frac{A_{k,m+1} - A_{k,m}}{\Delta T} \tag{13}$$

$$\frac{\partial^2 A(z,T)}{\partial T^2} = \frac{A_{k,m+1} - 2A_{k,m} + A_{k,m-1}}{\Delta T^2} \tag{14}$$

where $A_{k,m} = A(k\Delta z, m\Delta T)$. Substitute (12), (13), and (14) into (3)

$$\frac{A_{k+1,m} - A_{k,m}}{\Delta z} + \frac{j}{2}\left(\beta_2 + ig_0 T_2^2\right)\frac{A_{k,m+1} - 2A_{k,m} + A_{k,m-1}}{\Delta T^2} + \frac{1}{2}\left(g_0 - \alpha\right)A_{k,m} = j\gamma\left|A_{k,m}\right|^2 A_{k,m} \tag{15}$$

Therefore the field at $(z + \Delta z)$ can be calculated from the values of field at the preceding position z as follow

$$A_{k+1,m} = A_{k,m} + \Delta z\left[j\gamma\left|A_{k,m}\right|^2 A_{k,m} - \frac{j}{2}\left(\beta_2 + ig_0 T_2^2\right)\frac{A_{k,m+1} - 2A_{k,m} + A_{k,m-1}}{\Delta T^2} - \frac{1}{2}\left(g_0 - \alpha\right)A_{k,m}\right] \tag{16}$$

The process is repeated till the end of the fiber is reached. The output optical field then travels through the DSF. The same method is used to solve the Eq. (*1*) for getting the optical field at the end of the DSF.

The optical field output from the DSF is then filtered using the filter transfer function in Section 2.4. The filter is implemented in time domain as well. The filter output is calculated as follow

$$A_F = A_{DSF} * h(t) \tag{17}$$

Where A_F is the optical field at the output of the filter, A_{DSF} is the optical field at the output of the DSF, $h(t)$ is the pulse response of the filter function $H(f)$ and is determined using the Finite Impulse Response (FIR) technique [12].

The output of the filter is then multiplied with the modulator transmission function described in Eq. (7). The output is loop back to the input of EDFA and the calculation is repeated till the steady state is reached.

4 Results and discussion

4.1 Propagation of optical pulses in the fiber

Firstly, the fiber model is used to study the propagation of the pulses in an optical fiber. A *sech* profile pulse is launched into the fiber and the changes of the pulse along the traveling distance z are recorded. In the next two sections, the effects of dispersion and nonlinearity on the pulses are discussed.

4.1.1 Dispersion effect

The effect of GVD on the pulse propagation along an optical fiber is studied by setting other terms in Eq (*1*) to zero except the GVD term. The pulse envelope *A(z,T)* satisfies the following equation:

$$\frac{\partial A}{\partial z} = -\frac{j}{2}\beta_2 \frac{\partial^2 A}{\partial T^2} \qquad (18)$$

Figure 2 shows the simulation results for a hyperbolic-secant pulse with a full width at half maximum (FWHM) of 20 ps propagating in a standard single mode fiber (SMF) under GVD effect. Taking the value of the SMF's dispersion $D = 17\ ps/nm/km$ at 1550nm, β_2 can be calculated as: $\beta_2 = -21.7\ ps^2/km$.

It can be seen from Figure 2a that the pulses are broadened in temporal domain under GVD effect. Pulse width increases along the fiber and this broadening causes the pulse peak power drop by 65% at $z = 25km$. However there is no change in the pulse spectrum as seen in Figure 2b.

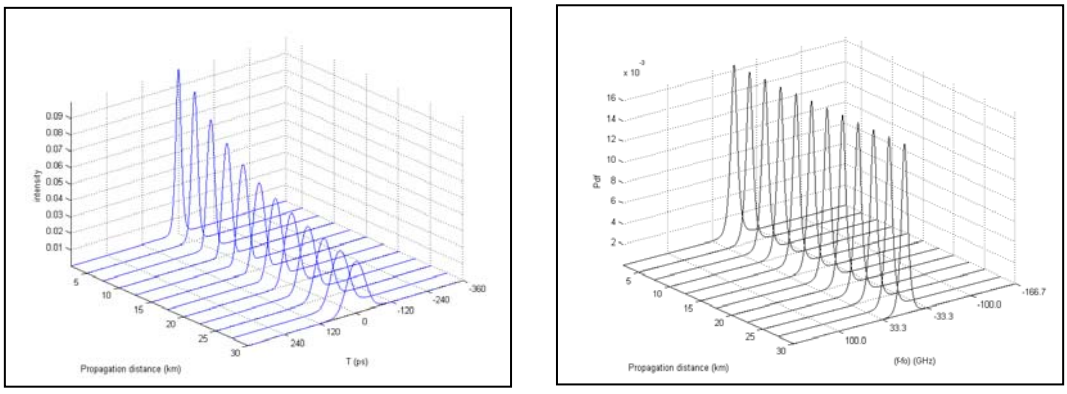

(a) **(b)**

Figure 2 - Hyperbolic-secant pulse propagation in a single mode fiber (SMF) under GVD effect in temporal domain (a) and in frequency domain (b); λ=1550nm, β_2=-21.7ps^2/km

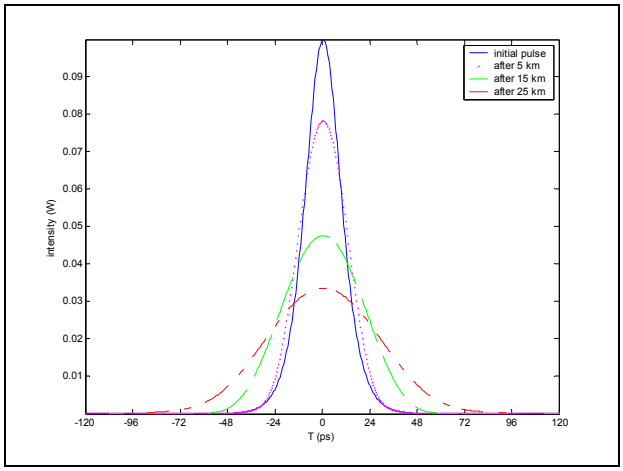

Figure 3 - Pulse broadening in SMF at z = 5km, 15km, and 25km

The pulse broadening at different traveling distances is illustrated in Figure 3. As the traveling distance increases the pulse width gets wider and the pulse peak power decreases. The pulse width is nearly double that of the initial pulse at $z = 25\ km$ and the peak power reduces to 35% of the initial value.

Propagation of the same pulse in a non-zero dispersion shifted fiber (NZ-DSF) is illustrated in Figures 4 and 5. The value of $\beta_2 = -3.82\ ps^2/km$ calculated from the dispersion value of $D = 3\ ps/nm/km$ at 1550nm for NZ-DSF.

Pulse broadening is less severe in NZ_DSF than in SMF. The pulse width (FWHM) just increases slightly after traveling a distance of 25 km to 21 ps. This can be understood by comparing the traveling distance to the dispersion length for the pulse when traveling in SMF and in NZ_DSF. The dispersion length is defined as

$$L_D = \frac{T_0^2}{|\beta_2|} \tag{19}$$

where T_0 is the *1/e* pulse width and related to the full width at half maximum T_{FWHM} as: $T_{FWHM} = 1.665T_0$.

For the pulse width of $T_{FWHM} = 20\ ps$, the dispersion lengths for SMF and NZ-DSF are 6.66 km and 37.7 km respectively.

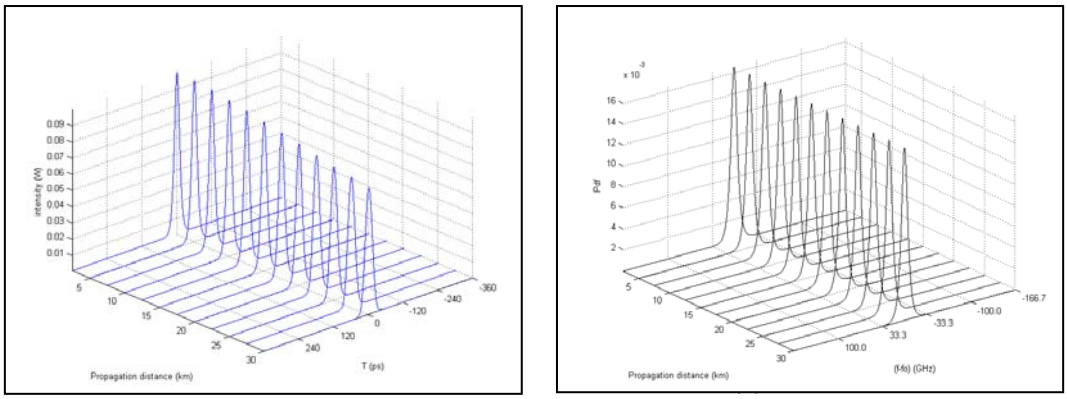

Figure 4 - Hyperbolic-secant pulse propagation in a non-zero dispersion shifted fiber (NS-DSF) under GVD effect in temporal domain (a) and in frequency domain (b); λ=1550nm, β_2=-3.82ps^2/km

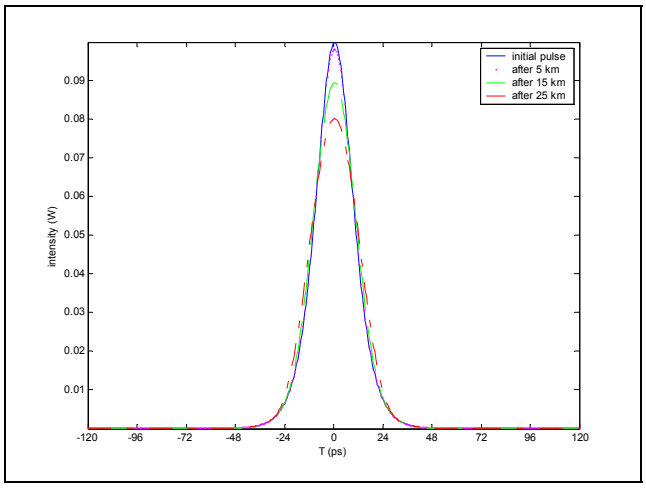

Figure 5- Pulse broadening in NZ-DSF at z = 5km, 15km, and 25km

4.1.2 Self phase modulation effect

The self phase modulation effect is studied by setting other terms in Eq (*1*) to zero except the SPM term. The pulse propagation is described by following equation

$$\frac{\partial A}{\partial z} = j\gamma |A|^2 A \qquad (20)$$

Figure 6 shows the propagation of a hyperbolic-secant pulse with the pulse width of $T_{FWHM} = 20\ ps$ and peak power of $P_0 = 0.1W$. The γ takes the typical value of $1.53W^{-1}km^{-1}$. There is no change in the temporal domain. The pulse shape and pulse width does not vary along the traveling distance. However, the pulse spectrum is spread out severely due to the phase shift induced by the SPM.

The spreading of the pulse spectrum is illustrated clearly in Figure 7, in which the pulse spectrums at different traveling distances are plotted. The pulse spectrum gets wider as the pulse propagates along the fiber. The two peaks appear at $z = 25\ km$. This is consistent with the results in [6], where the nonlinear Schrodinger equation is solved analytically. There are two peaks in the pulse spectrum at $\xi = 4.5$, where ξ is the normalized propagation length and is defined as

$$\xi = z/L_{NL} \tag{21}$$

with z is the propagation length, L_{NL} is the nonlinear length

$$L_{NL} = 1/\gamma P_0 \tag{22}$$

Using $\gamma = 1.53\ W^{-1}km^{-1}$ and $P_0 = 0.1\ W$, the nonlinear length is $L_{NL} = 6.54\ km$. The normalized propagation length for $z = 25\ km$ is $\xi = 3.8$.

The pulse spectrum broadening is also studied with different values of γ and P_0. The results are plotted on Figures 8 and 9. Pulse spectrum broadening at $z = 25\ km$ decreases as γ decreases or P_o decreases.

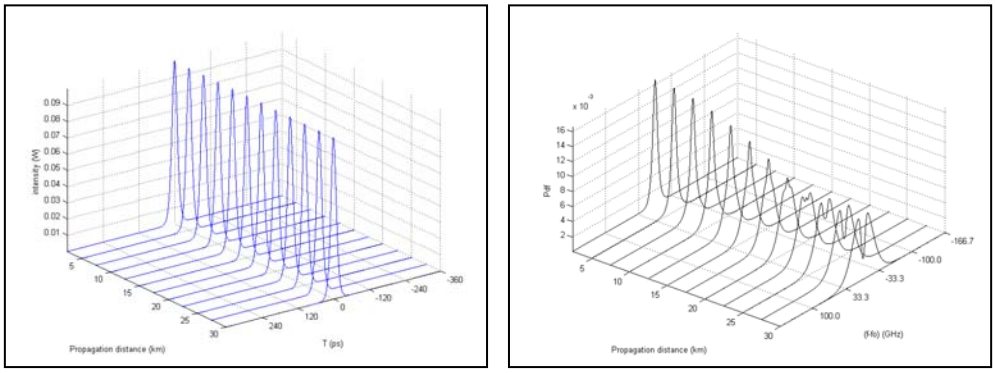

(a) **(b)**

Figure 6 - Hyperbolic-secant pulse propagation in a single mode fiber (SMF) under SPM effect in temporal domain (a) and in frequency domain (b); λ=1550nm, γ=1.53W^{-1}km^{-1}

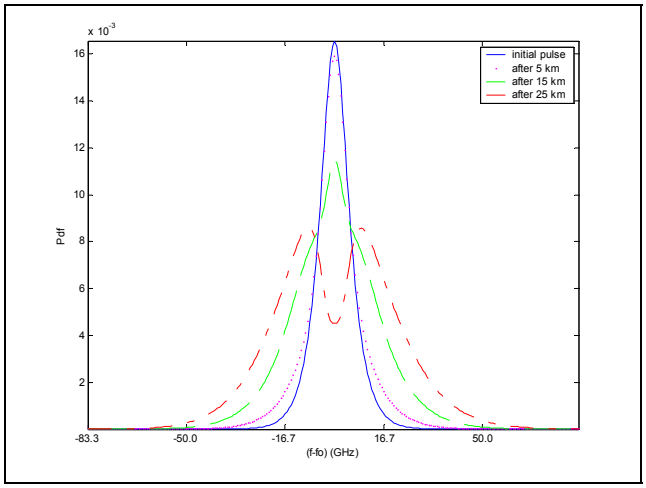

Figure 7 - Pulse spectrum broadening at z = 5km, 15km and 25km

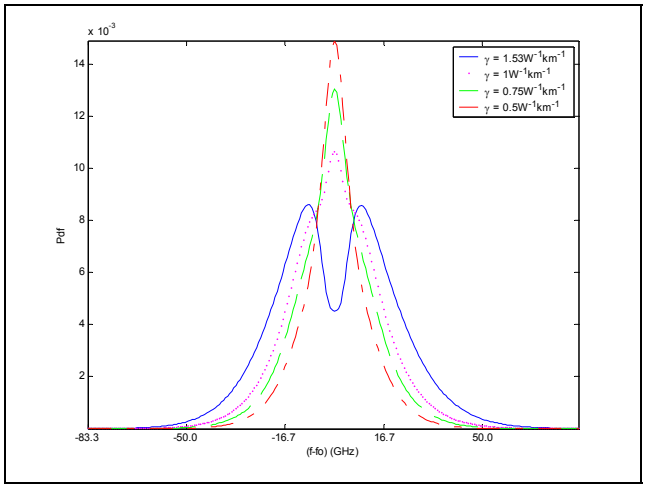

Figure 8 - Hyperbolic-secant pulse spectrum after propagating a distance of z = 25km for different values of γ

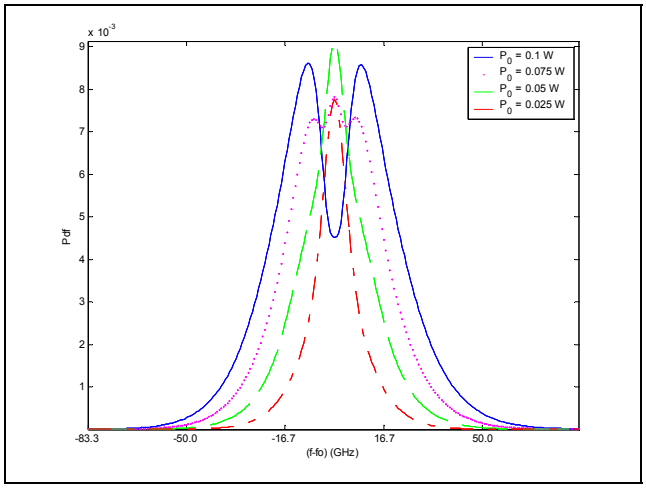

Figure 9 - Hyperbolic-secant pulse spectrum after propagating a distance of z = 25km for different values of peak power P_0.

4.1.3 Combine effect of GVD and SPM effect, soliton pulse

The equation for the pulse propagation under GVD and SPM effects is

$$\frac{\partial A}{\partial z} = -\frac{j}{2}\beta_2 \frac{\partial^2 A}{\partial T^2} + j\gamma |A|^2 A \qquad (23)$$

The soliton theory shows that when a hyperbolic-secant pulse with the pulse width T_o and peak power P_o satisfy the condition $T_0^2/|\beta_2| = 1/\gamma P_0$ launched into the fiber, the GVD and SPM effects will balance each other and hence the pulse will propagate without any change in its pulse shape and spectrum.

Figure 10 shows simulation result of the propagation of a hyperbolic-secant pulse in a SMF. The pulse width is $T_{FWHM} = 20$ ps ($T_o = 12$ ps) and the peak power is $P_0 = 0.1$ W. Therefore the soliton condition is satisfied and hence the pulse shape as well as pulse spectrum keeps unchanged when the pulse propagates along the fiber as seen in Figure 10.

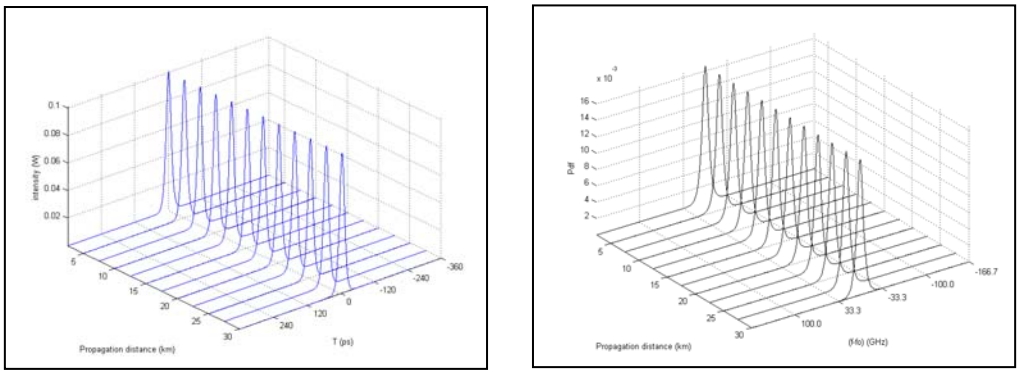

(a) **(b)**

Figure 10 - Hyperbolic-secant pulse propagation in a single mode fiber (SMF) under GVD and SPM effects in temporal domain (a) and in frequency domain (b); λ=1550nm, γ=1.53W^{-1}km^{-1}, β_2=-21.7ps^2/km, P_0=0.1W, T_{FWHM}=20ps

4.2 Harmonic mode-locked fiber laser

4.2.1 Mode-locked pulse evolution

The laser model is as described in Section 2. Unlike other simulations on the mode-locked fiber laser reported so far [11, 13], which are solely based on split-step Fourier method for solving the nonlinear Schrodinger (NLS) equation and simulate only one pulse in the ring, the method simulation reported here is modeled fully in time domain and hence there is no need to convert the pulses into frequency domain. This makes

the model can simulate not just one pulse but all pulses traveling in the ring, which actually happens in harmonic mode-locked ring laser.

The laser is excited from a flat amplitude initial line, which is regarded as a continuous wave. After about 3000 round trips, steady state output harmonic mode-locked pulses are reached as shown in Figure 11. It can be seen that there are 4 pulses exist in one time period of the ring as the modulation frequency is set to be 4 times the ring frequency. The laser is locked to the 4^{th} harmonic. The ring period is the time required for the pulses propagate a round trip and calculated from the lengths of the fibers (0.1 m of EDF and 2 m of DSF) with assumption that there is no delay induced by other components such as modulator and filter. The lengths of the fibers are chosen to be short to reduce the simulation time. The insertion losses of the modulator and filter are set to zero to minimize the total loss of the cavity. The other settings for the ring are: amplification factor $g_{ss} = 3$, saturation power $P^{sat} = 10\ mW$, filter bandwidth $BW_f = 400\ GHz$ ($0.32\ nm$), modulation depth $\Delta_m = 0.5$, modulation frequency $f_m = 0.39GHz$ (the 4^{th} harmonic of the ring frequency), the dispersion of the EDF and DSF at 1550nm are *17 ps/nm/km* and *3 ps/nm/km* respectively, the nonlinear parameters of both fibers are $1.53\ W^{-1}km^{-1}$.

The close look of the mode-locked pulses and its spectrum are shown in Figure 12.

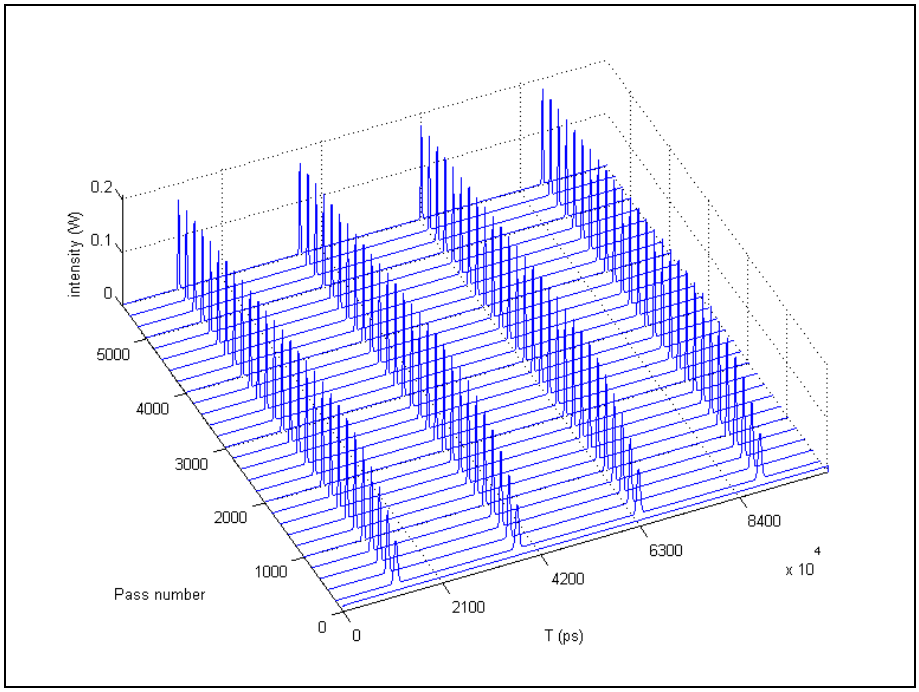

Figure 11 - Pulse evolution in a harmonic active mode-locked fiber laser, 4 pulses traveling in the ring for the fourth harmonic order. The pass number indicates the number of pass though the ring laser.

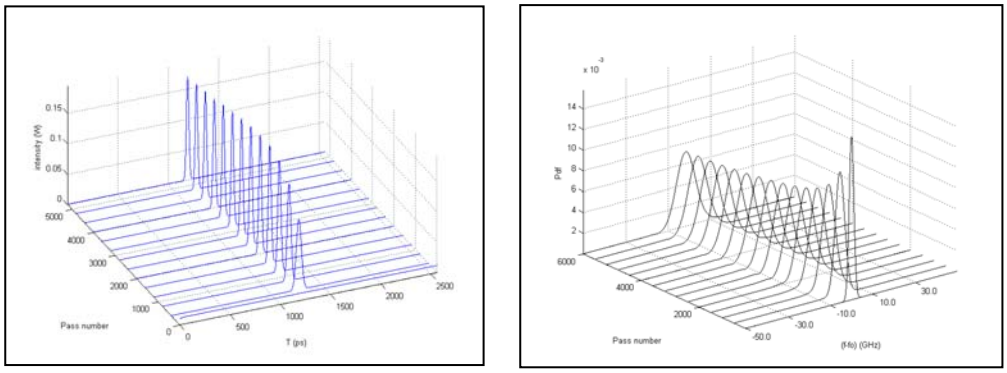

(a) **(b)**

Figure 12- Pulse evolution in an active harmonic mode-locked fiber laser, (a) temporal domain, (b) frequency domain

4.2.2 Effect of modulation frequency

The effect of modulation frequency on the mode-locked pulses is studied by running the simulation with different values of modulation frequency. Other settings of the laser are the same as previous.

Steady-state pulses and their spectrums with modulation frequencies of 0.39 GHz, 0.78 GHz, 1.16 GHz and 2.32 GHz (corresponding to the 4^{th}, the 8^{th}, the 12^{th} and 24^{th} harmonic of the ring frequency/fundamental frequency $f_F = 97.6\ MHz$) are plotted in Figure 13.

The peak power of the pulses reduces as the modulation frequency increases. This is consistent with the energy conservation. As the modulation increases more pulses traveling in the rings and they are sharing the same energy provided by the pump signal in one ring period. The energy provided by the pump in one ring period is constant, as the pump power is kept unchanged. When the number of the pulses, which are traveling simultaneously in the ring, increases the total energy is divided among those pulses and hence each pulse accumulates less energy.

The steady-state pulse train's pulse width and bandwidth are plotted against modulation frequency in Figure 14. As the modulation frequency increases 4 times, the pulse width decreases to a half and the bandwidth is double. The simulation results show that the bandwidth increases proportional to the square root of modulation frequency while the pulse width decreases proportional to square root of modulation frequency. Therefore higher modulation frequency not only produces pulses with higher repetition rate but also makes the pulses shorter. This is consistent with the experiment results shown in [14]. However, as discussed above, the modulation frequency cannot increase infinitely but is limited by the bandwidth of the modulator. The higher repetition rate can be obtained by detuning technique, which will be simulated and discussed in details in Section 4.3.

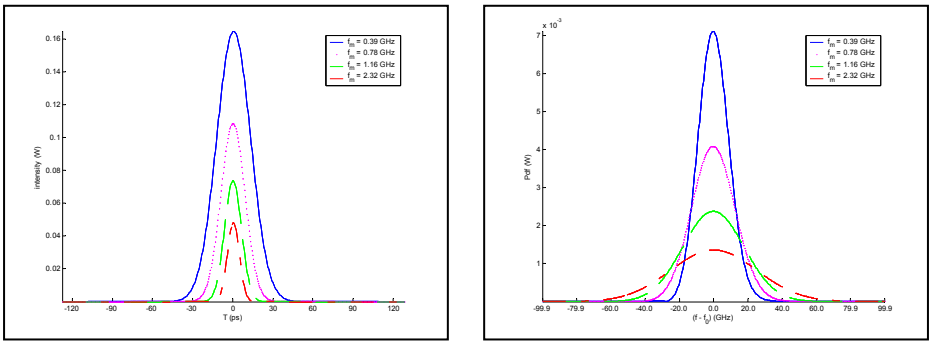

(a) **(b)**

Figure 13 - Mode-locked pulses with different modulation frequencies, (a) temporal domain, (b) frequency domain

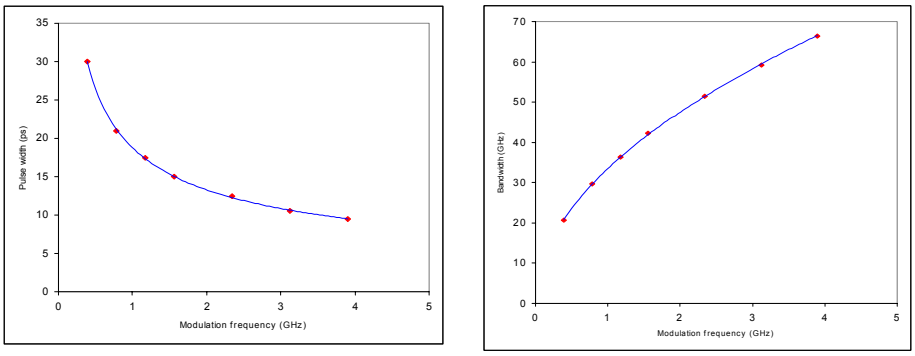

(a) **(b)**

Figure 14 - Pulse width and bandwidth as a function of modulation frequency

4.2.3 Effect of modulation depth

In this section, the effect of modulation depth is examined by studying the laser output under different settings of modulation depth Δ_m. The pulse evolutions with $\Delta_m = 0.5$, $\Delta_m = 0.2$, and $\Delta_m = 0.1$ are shown in Figures 15, 16, and 17. The modulation frequency is $f_m = 1.56$ GHz. Other settings are the same as earlier discussion.

The simulation result shows that with the decrease of modulation depth, the damped oscillation process during pulse evolution is last longer. This can be easily explained by comparing these simulated with experimental results. Deeper modulation depth shapes the pulse effectively and mode-locking process is enhanced. However, there is only a slight difference in both the pulse width and bandwidth when the pulses reach the steady state as shown in Figures 18 and 19.

When the modulation depth is reduced to *0.001 (or 0.1%)*, no mode-locked pulse is generated. This is the modulation depth threshold for mode locking. This value is quite different to the threshold obtained from experiment, where the threshold value of modulation depth is found to be *0.08* [14]. The difference may be due to the noise and environmental conditions in the experiment set-up which are not included in our simulation model.

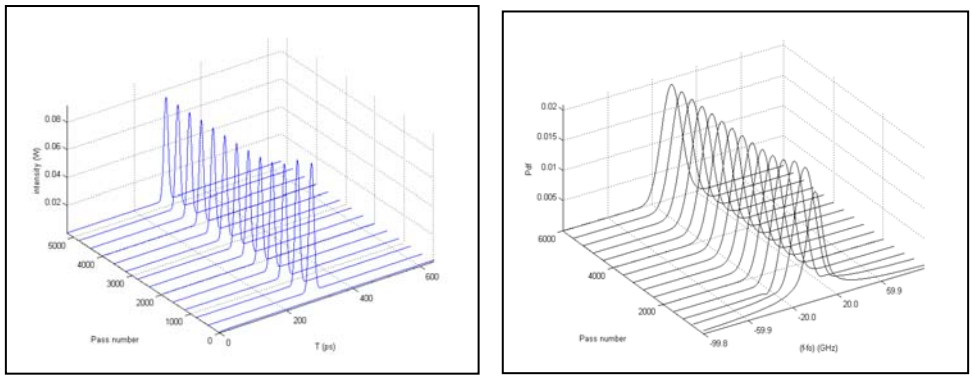

Figure 15 - Pulse evolution in temporal domain (a) and frequency domain (b) under modulation depth of 0.5

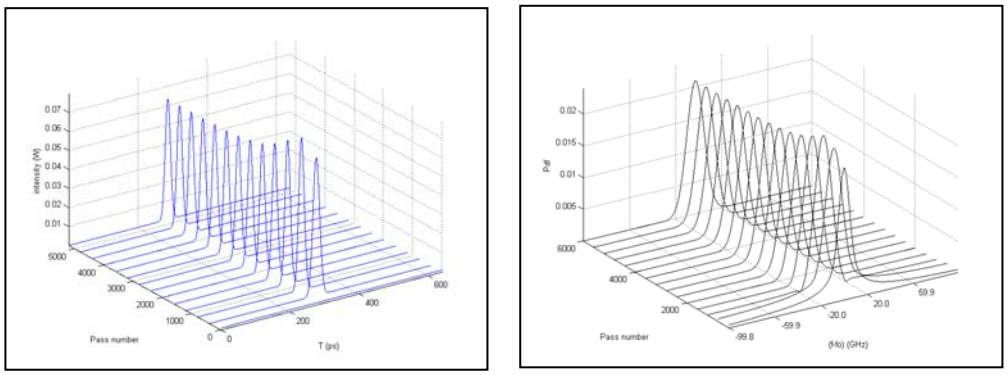

(a) **(b)**

Figure 16 - Pulse evolution in temporal domain (a) and frequency domain (b) under modulation depth of 0.2

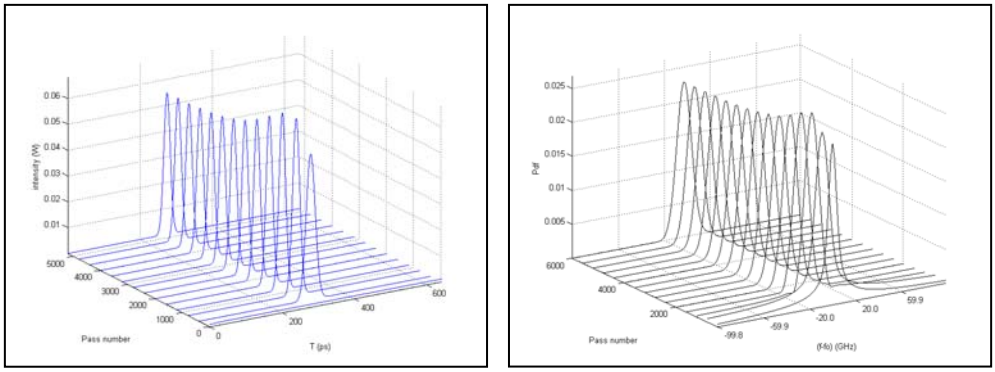

(a) **(b)**

Figure 17 - Pulse evolution in temporal domain (a) and frequency domain (b) under modulation depth of 0.1

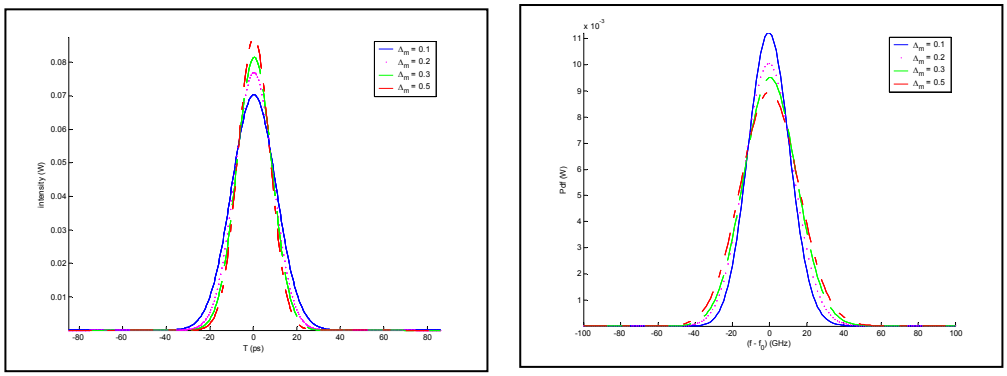

(a) **(b)**

Figure 18 - Mode-locked pulses with different modulation depths, (a) temporal domain, (b) frequency domain

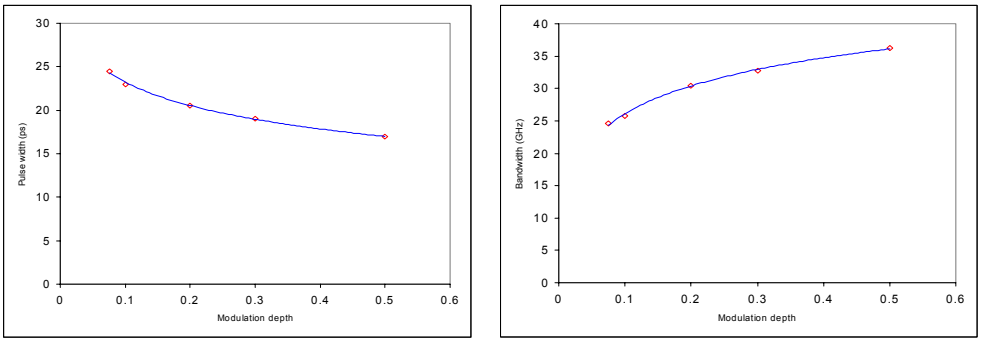

(a) **(b)**

Figure 19 - Pulse width and bandwidth as a function of modulation depth

4.2.4 Effect of the optical filter bandwidth

The filter is inserted into the laser cavity to select the central wavelength and help to shape the pulse. As the pulse pass through the modulator on every round trip, it is compressed in temporal domain and spread in frequency domain due to the sidebands induced by the modulation. However, the pulse cannot be compressed endlessly. The filter bandwidth will limit the pulse spectrum width and thus balances the temporal domain pulse compression. In this section, the mode-locked pulses are studied with variation of the filter bandwidth. The cavity settings are the same as before except that the filter bandwidth is varied. The simulation results are shown in Figures 20 and 21.

Figure 20 shows the steady-state pulses for various values of the filter bandwidth. Cavity with wider filter bandwidth generates pulses with narrower pulse width and wider bandwidth, and vise versa. As the filter bandwidth increases the pulse width becomes shorter with higher peak power. On the other hand, the pulse bandwidth increases with wider filter bandwidth.

Pulse width and bandwidth are plotted against the filter bandwidth in Figure 21. The pulse width decreases exponentially with the increase of filter bandwidth. Therefore, wider filter bandwidth is preferred as it generates shorter pulse. However in practice, mode locking is easier to obtain with narrow filter bandwidth. The laser is more difficult to be locked when the filter bandwidth is so wide because neither center frequency selection nor super-mode filtering obtained with a wide bandwidth filter.

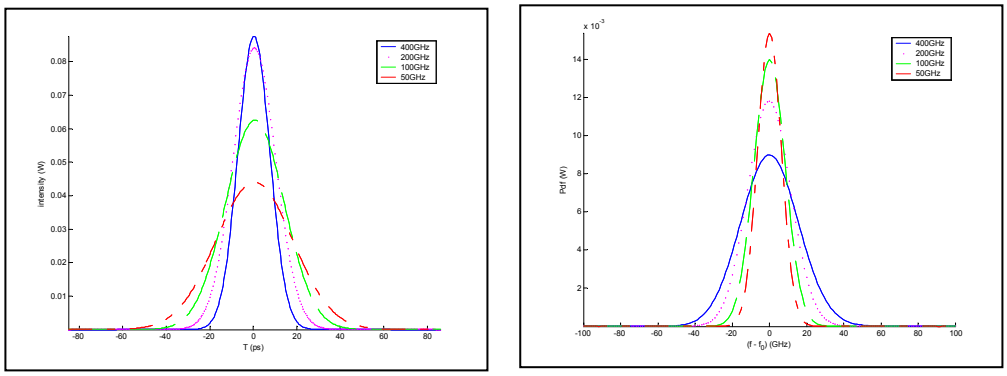

(a) **(b)**

Figure 20 - Mode-locked pulses with different filter bandwidths, (a) temporal domain, (b) frequency domain

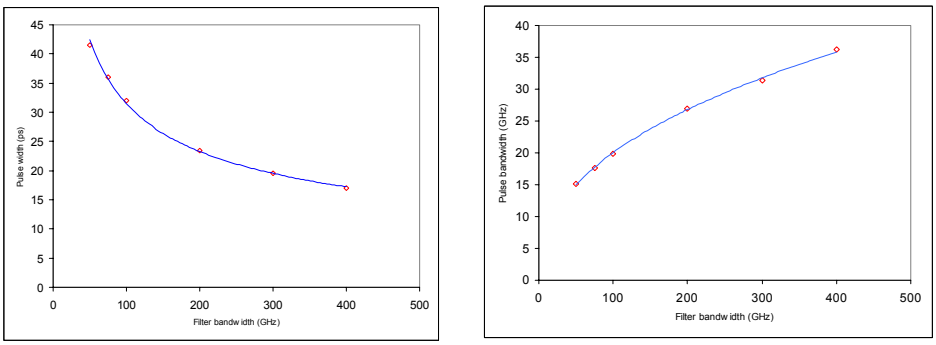

(a) **(b)**

Figure 21 - Pulse width and bandwidth as a function of filter bandwidth

4.2.5 Effect of pump power

The effect of the pump power on the mode-locked pulses is also studied by varying the values of P^{sat} in the EDFA model and keeping other settings the same.

Figure 22 shows the mode-locked pulses for various values of P^{sat}. When P^{sat} varies, only the peak power of the pulses is affected while the pulse width and bandwidth is nearly unchanged. This is consistent with the result obtained in experiment. The pulse width and bandwidth do not vary with the change of the pump power in the short length ring setup. The shortening of the pulse due to the increase of the pump power is just observed when the length of the ring is 118 m [14].

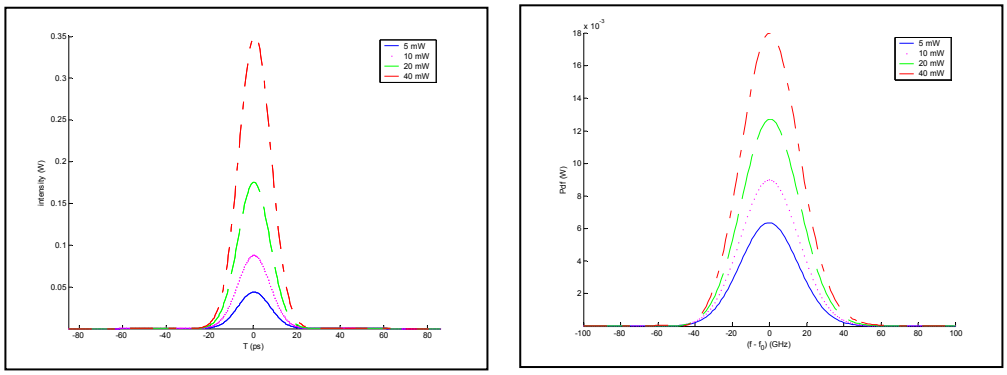

(a) **(b)**

Figure 22 - Mode-locked pulses with different values of P^{sat}, (a) temporal domain, (b) frequency domain

4.3 Rational harmonic mode-locked fiber laser

As discussed above, the repetition rate of the active mode-locked laser is limited by the bandwidth of the modulator. To increase the repetition rate, rational harmonic mode-locking (RHML) technique is applied. In RHML laser, the modulation frequency is not an integer number harmonic of the fundamental frequency f_R but detuned by an amount of f_R/N

$$f_m = mf_R + f_R/N \qquad (24)$$

where m *and* N are integer numbers and N is defined as the multiplying factor. The output pulse repetition rate is now no longer f_m but Nf_m. In another word, the repetition rate has been multiplied by a factor of N.

The cavity settings are the same as before, except that the modulation depth is $\Delta_m = 0.1$, and the gain factor is $g_{ss} = 6$. The higher gain factor is required because in RHML the pulses do not pass the modulator at the minimum loss position but at different loss positions for every round trip. Therefore the pulses in RHML experience more loss

than that of HML and hence require higher gain to compensate for the loss. When the modulation frequency is set to *0.39 GHz*, which corresponds to the 4th of the fundamental frequency f_F = *97.6 MHz*, harmonic mode-locking is obtained with 4 pulses traveling in the ring as shown in Figure 23

When the modulation frequency is detuned by $f_F/2$ to become *0.439 GHz*, doubling repetition rate has been obtained as shown in Figure 24. It can be seen that there are totally 9 pulses traveling in the ring during one ring period T_R. It is interesting that the amplitude-unequal pulses are also observed. This again confirms the experimental result that RHML can be used to increase the repetition rate but the output pulses suffer amplitude fluctuating from pulse to pulse unless pulse amplitude equalization is applied.

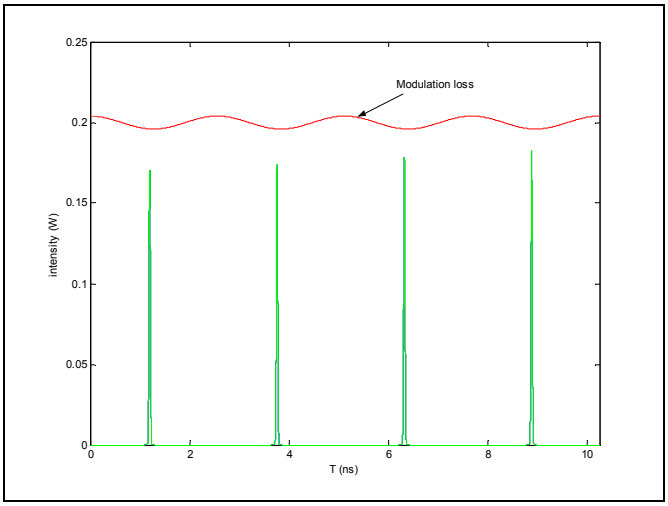

Figure 23 – Harmonic mode-locking with 4 pulses in one ring period T_R when the modulation frequency is set to 4 times the fundamental frequency

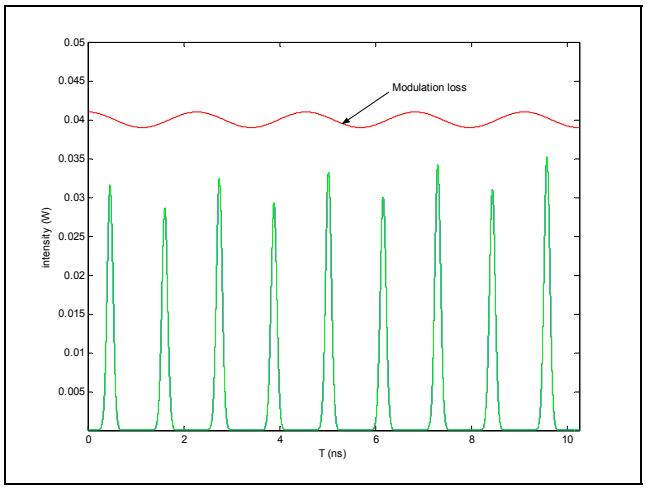

Figure 24 – Rational harmonic mode-locking with 9 pulses in one ring period T_R when the modulation frequency is set to 4.5 times the fundamental frequency

5 Conclusions

A novel temporal domain approach has been developed to simulate the generation and propagation of photonic pulses in mode-locked lasers and presented in this paper. The pulse propagation equation has been solved fully in both time and spatial domain using finite difference method without the need of conversion of optical signals into frequency domain unlike other published works that employed the split-step Fourier method [6, 8]. This approach allows simulation of not just only one pulse but the whole pulse train generated in the harmonic mode-locked fiber laser. To the best of our knowledge this simulation is developed for the first time.

In summary this paper presents the followings: firstly, the propagation of an optical pulse inside a fiber has been simulated to ensure the validity of our numerical approach. Propagation of lightwave pulses has been tested and compared when the fiber is under linear and nonlinear operating conditions, that is under the linear dispersion effect and/or under the self-phase modulation effect. It is noted that only the SPM effect is included in this simulator. Other nonlinear effects such as Raman scattering and four wave mixing effects can be easily incorporated without difficulty. It is found that GVD and SPM play important roles in the propagation of the pulse. Under GVD effect, different chromatic components of the fiber travel with different velocity and that causes the pulse spread out in temporal domain while its spectrum keeps unchanged. On the other hand, phase shift induced by the SPM effect widen the pulse spectrum while keeping the pulse shape in temporal domain unchanged. When the two effects work together on a hyperbolic-secant pulse, their effects cancel each other and the result is that the pulse shape and spectrum keep unchanged while the pulse propagates inside the fiber.

The pulse formation in a harmonic mode-locked fiber laser has been simulated. The formation of N mode-locked pulses traveling in the ring when the laser is locked to the N^{th} harmonic has been demonstrated in our simulation technique. The effects of the modulation frequency on the output pulse characteristics such as pulse width and bandwidth have also been studied. The pulse width decreases inverse proportionally while the bandwidth increases linearly with the square root of modulation frequency. The effect of modulation depth on the output pulses has also been examined. It is found that as the modulation depth increases the pulse width slightly decreases and

the bandwidth increases a little. The filter bandwidth has been found to have great effect on the pulse width and bandwidth. The pulse width decreases exponentially with an increase of the filter bandwidth. Hence wider filter bandwidth is preferred for shorter pulse generation. However, in practice the fiber laser can be easily locked using narrow filter bandwidth than with the wider one.

The output pulse characteristic has also been examined with the variation of the pump power. As the pump power increases the output pulse power increases but the pulse width and bandwidth remain the same. This is consistent with the experiment result that the pump power does not affect to the pulse width and bandwidth as the fiber ring length is short compared to the nonlinear length of the fiber.

Finally rational harmonic mode-locking has been demonstrated. By detuning the modulation frequency to a half of the fundamental frequency, doubling repetition rate has been realized. Simulation results of rational harmonic mode-locking have been demonstrated with the multiplication of the repetition rate of the mode-locked pulse trains. However there is amplitude fluctuation in the output pulses and hence amplitude equalization should be employed in the RHML laser.

References

[1] H. C. Bao, H. F. Liu, and Y. J. Wen, "Amplitude noise of 40-GHz pulses from a subharmonically synchronous mode-locked semiconductor laser," *Photonics Technology Letters, IEEE*, vol. 14, pp. 540-542, 2002.

[2] G. Lin, J. Wu, and Y. Chang, "40 GHz rational harmonic mode-locking of erbium-doped fiber laser with optical pulse injection," presented at Optical Fiber Communications Conference, 2003. OFC 2003, 2003.

[3] M. Nakazawa and E. Yoshida, "A 40-GHz 850-fs regeneratively FM mode-locked polarization-maintaining erbium fiber ring laser," *Photonics Technology Letters, IEEE*, vol. 12, pp. 1613-1615, 2000.

[4] T. Pfeiffer and G. Veith, "40 GHz pulse generation using a widely tunable all-polarisation preserving erbium fibre ring laser," *Electronics Letters*, vol. 29, pp. 1849-1850, 1993.

[5] D. L. A. Seixas and M. C. R. Carvalho, "50 GHz fiber ring laser using rational harmonic mode-locking," presented at Microwave and Optoelectronics

Conference, 2001. IMOC 2001.Proceedings of the 2001 SBMO/IEEE MTT-S International, 2001.

[6] G. P. Agrawal, *Nonlinear Fiber Optics*, 2001.

[7] J. R. Costa, C. R. Paiva, and A. M. Barbosa, "Modified split-step Fourier method for the numerical simulation of soliton amplification in erbium-doped fibers with forward-propagating noise," *Quantum Electronics, IEEE Journal of*, vol. 37, pp. 145-152, 2001.

[8] G. P. Agrawal, *Applications of Nonlinear Fiber Optics*, 2001.

[9] A. M. Gomilko, A. A. Gourjii, V. B. Katok, and V. G. Levandovskyy, "Investigation of pair optical soliton propagation in dispersion managed fiber link with two numerical methods," presented at Transparent Optical Networks, 2001. Proceedings of 2001 3rd International Conference on, 2001.

[10] T. Kaczmarek, "Propagation of chirped ultra-short optical pulses," presented at Transparent Optical Networks, 1999. International Conference on, 1999.

[11] G. Sluyterman and L. U. Ropke, "Comparison of numerical simulation of a polarization-maintaining figure-eight laser with experiment," presented at Lasers and Electro-Optics, 1999. CLEO '99. Summaries of Papers Presented at the Conference on, 1999.

[12] C. I. Emmanuel and W. J. Barrie, "Digital Signal Processing A Practical Approach," 1993.

[13] E. Marti-Panameno, J. J. Sanchez-Mondragon, and V. A. Vysloukh, "Theory of soliton pulse forming in an actively modelocked fiber laser," *Quantum Electronics, IEEE Journal of*, vol. 30, pp. 822-826, 1994.

[14] Q. H. Lam and N. B. Le, "Implementation and characterization of active harmonic mode-locked fiber lasers," Monash university, Technical report 2004.